Journal of Statistical Physics, Vol. 95, Nos. 5/6, 1999

Dynamics of Faceted Grain Boundary Grooves

J. G. Dash,[1] V. A. Hodgkin,[1] and J. S. Wettlaufer[1, 2]

Received July 28, 1998; final September 24, 1998

The dynamics of dislocation-free crystal facets is examined in the context of grain boundary grooves at the junction between two crystallites of a solid and the liquid phase. The geometry and thermal conditions of grain boundary grooves allow a detailed analysis of facet morphology during solidification in terms of the nucleation and spreading rates of elementary crystal planes. Observations on the freezing of water in a two-dimensional cell reveal several dynamical features which are treated by the theory. Additional observations provide indications for the stiffness and premelting of grain boundaries.

KEY WORDS: Nucleation; surface free energy; facets; grain boundaries; crystal growth.

1. INTRODUCTION

The interface between a polycrystal and its melt liquid is indented by grooves at the triple junctions between two grains and the liquid. Under isothermal conditions the depth and shape of a groove are determined by the relations between the three interfacial coefficients. The shape is modified by the imposition of a temperature gradient,[1, 2] an effect which forms the basis for a technique of measuring the solid–liquid interfacial energy.[3, 4] Typical grooves have smoothly rounded sides emerging from sharp clefts, but abrupt changes of slope can result from anisotropy of the crystal–melt surface tension.[5] An extreme case of fully faceted grain boundary grooves has been observed in ice-water interfaces.[6] In this paper we extend the work on faceted grooves to a study of their dynamics, and show how the rates of nucleation and spreading of elementary layers of the crystal are reflected in changes of shape and size of the grooves.

[1] Department of Physics, University of Washington, Seattle, Washington 98195.
[2] Applied Physics Laboratory, University of Washington, Seattle, Washington 98195.

0022-4715/99/0600-1311$16.00/0

The theory of crystal growth describes the temperature dependence of the growth of singular surfaces. Singular surfaces are those for which the surface free energy as a function of orientation has a pointed minimum. Such surfaces can spread parallel to the crystal plane as a continuous function of temperature, but growth in the normal direction requires supercooling in order to nucleate new crystal planes.[7] The original formulation assumed that nucleation is necessary only for sharp interfaces, and that diffuse interfaces could grow in the normal direction without supercooling. John Cahn[8] elaborated the theory to treat diffuse and non-singular surfaces, and showed that even diffuse surfaces require a finite driving force for growth normal to their planes. In a subsequent paper Cahn, Hillig and Sears[9] extended the theory and applied it to experimental results on a number of materials, including ice.[10]

In the present work we adapt the theory to treat faceted grain boundary grooves, and show how the shape and size of the grooves are systematically related to the rate of nucleation and spreading of individual layers. The analysis is applied to experiments on the freezing of water in a two-dimensional cell.

2. TYPICAL GRAIN BOUNDARY GROOVES

Grain boundary grooves at a solid–melt interface are analogous to the meniscus of a liquid that wets the wall of a vessel. The liquid rises to a certain height L to reduce the surface energy by an amount proportional to ΔEL, where ΔE is the difference between the surface energies of the wall when dry and wet. The rise is opposed by gravitational energy. In the case of a solid–melt interface, the groove is caused by the difference between the solid–liquid interfacial energy and the grain boundary energy between the two crystallites, $\Delta\gamma$. In place of gravitational energy, the depth is opposed by the free energy difference between the crystal and the supercooled liquid within the groove. Typical grooves have rounded faces and depth given by

$$L = (\Delta\gamma T_o/q\,\nabla T)^{1/2} \tag{1}$$

where T_o is the melting temperature, q is the latent heat of fusion per unit mass and ∇T is the gradient within the liquid filling the groove.

Hardy[4] studied grain boundary grooves in ice to determine the interfacial energy of the ice-water interface. Wilen and Dash[6] recently studied grain boundary grooves at an ice-water interface in a radial, two-dimensional geometry. They found that most of the grooves were of typical rounded shape, and had depths consistent with estimates based on Eq. (1). However, a fraction were much deeper, with straight sides, such as

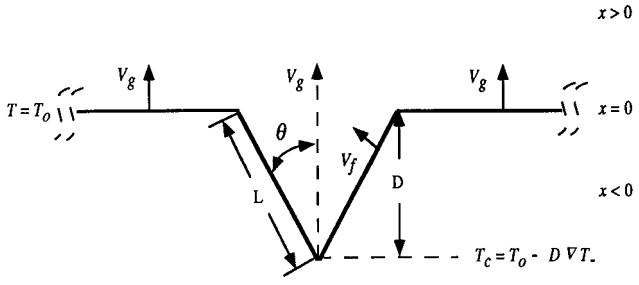

Fig. 1. Schematic of a faceted groove.

illustrated in Fig. 1. In this paper we study the dynamical changes of faceted grooves in terms of the nucleation of elementary crystal layers.

3. ORIGIN AND DYNAMICS OF FACETED GROOVES

Faceted grooves result from certain textures of crystal grains at a solid–liquid interface, where the orientations of singular crystal surfaces are tangent to the curved faces of a normal grain boundary groove. In such a groove the singular facets can elongate continuously with temperature parallel to the surface, but they cannot advance in the direction normal to the surface until a portion of their surface is supercooled to the nucleation temperature. When a temperature gradient is applied to the groove, causing the overall interface to advance, the groove deepens, with spreading faces of singular facets, but their normal growth is pinned until the groove depth is sufficient to lower the cleft temperature to the critical value. When this occurs new layers are nucleated at the cleft, where the grain boundary makes contact with the edge of the facet. As new layers are created the groove can advance with the interface, as long as the continued nucleation and spreading of the layers can keep pace with the interface. The general features of a faceted groove are shown in Fig. 1.

Nucleation is most rapid in the cleft, where the temperature is lowest, and monolayers created there spread outward toward the interface. At low freezing rates each layer can spread completely across the groove before the next layer is nucleated, so that the surface never has more than one incomplete layer. At higher freezing rates the surface has several steps, so that the surface is not perfectly parallel to a principal direction. The groove shape evolves smoothly, from fully single-faceted sides, to a combination of shorter facets and curved sections.

The evolution is analyzed in terms of the model illustrated in Fig. 1. Ice fills the half space at $x<0$ (except for the groove), while water extends

through $x > 0$. In steady state conditions the boundary at T_o proceeds at constant speed V_g in the $+x$ direction, under the impetus of the uniform temperature gradients ∇T_- $(x < 0)$ and ∇T_+ $(x > 0)$. In this regime the groove shape is predicated on the assumption that the time τ_p for a layer to spread parallel to its surface is short compared to the average time τ_n to nucleate a new layer, so that each step crosses the surface completely before the next layer is nucleated.

The faceted groove translates with the advancing interface by the nucleation of the layers on each side of the groove. The nucleation time is related to the speed V_g of the bulk interface and the growth rate normal to the facet V_f by:

$$V_g \sin\theta = V_f = h/\tau_n \tag{2}$$

where h is the thickness of an elementary layer and θ is the inclination of the facet with respect to the x direction.

We consider two cases for the nucleation frequency in this geometry. According to classical nucleation theory[8, 10, 11] the nucleation rate J depends exponentially on the activation energy of a critical-sized pillbox with free energy ΔG^*:

$$J = 1/\tau_n = A \exp[-\Delta G^*/k_b T]; \qquad \Delta G^* = \pi\lambda^2 T/nq(T_o - T_c) \tag{3}$$

where λ is the line tension of the edge between a layer of solid and liquid, n is the two-dimensional density, q is the latent heat of fusion per unit mass, T_o and T_c are the temperatures at the bulk phase boundary and at the cleft, and the prefactor A is the initial growth rate of a critical nucleus.[3]

For the temperature gradients under consideration, we ignore the curvature of the isotherms within the cleft and assume a constant linear temperature gradient along the facet, $G = \cos\theta \nabla T_-$ so that the temperature is written as $T(z) = T_o - Gz$, where the z coordinate is parallel to the facet plane with the origin located where the facet intersects the bulk interface at T_o. The maximum undercooling is at the cleft, where $T(L) = T_c$. The nucleation frequency $1/\tau_n$ of two-dimensional islands of monomolecular height varies with temperature and hence position along the facet. The probability of nucleation thus varies according to

$$p(z) = A \exp[-\pi\lambda^2/k_b nq(T_o - T(z))] \tag{4}$$

[3] We note here that in the general theory of nucleation, the prefactor is a quantity of considerable difficulty to measure and to describe theoretically even when invoking rather gross assumptions. Experiments with dislocation free Ga crystals indicate that A is proportional to $(T_o - T_c)^M$, where M depends on the facet (see e.g., Pennington[12]). However, Hillig[10] finds little evidence for such a dependence on basal plane facets of ice. Therefore, we treat it as a constant.

and therefore V_f depends on the length averaged probability distribution along the facet;

$$\frac{1}{\tau_n} = \frac{1}{L}\int_0^L p(z)\,dz = \frac{A}{L}\int_0^L \exp\left[-\frac{c}{z}\right] dz \tag{5}$$

where $c = \pi\lambda^2/k_b nqG$. A change of variable $y = L/z$ leads to the solution

$$V_f = hA\left[\exp(-c/L) - \frac{c}{L}E(c/L)\right] \tag{6}$$

where $E(y)$ is the exponential integral. Under the assumption that nucleation only occurs at one temperature T_c, the rate depends only on the first term of Eq. (6). At this stage we can understand how the overall growth rate V_g and the groove depth $D = L\cos\theta$ are related. In Fig. 2 we plot $V_g \sin\theta$ as a function of the groove depth for both cases described by Eq. (6). The undercooling and hence nucleation rate at constant gradient must increase with groove depth which must result in an increase in the overall growth rate within this type of model. Note the more rapid rise in growth rate with groove depth in the case where the spatial variation in the nucleation temperature is considered.

The speed of advance of the interface at T_o is governed by the gradients in the ice and water, which control the dissipation of latent heat from the boundary. The net heat flux balance per unit area across the interface is

$$\rho_i q V_g = (k_i \nabla T_- - k_w \nabla T_+) \tag{7}$$

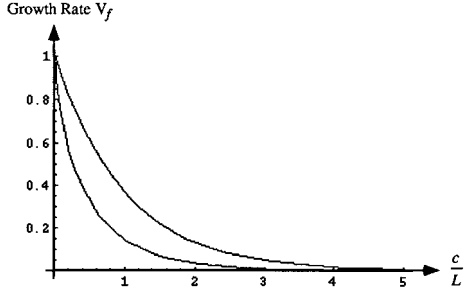

Fig. 2. The growth rate $V_g \sin\theta = V_f$ as a function of the groove depth for both cases described by Eq. (6). The upper curve assumes that nucleation occurs only at the cleft of the groove, hence is a pure exponential. The lower curve allows for the extension of nucleation probability over a finite distance above the cleft, as given by Eq. (6). Note the more rapid rise in growth rate with groove depth in the case where the spatial variation in the nucleation temperature is considered.

where ρ_i is the density of ice, and k_i and k_w are the thermal conductivities of ice and water, respectively. The depth D of the groove can be related to the temperature gradient and the speed of the interface. Since the temperature at the cleft $T_c = T_o - D\,\nabla T_- = T_o - GL$, we can express the supercooling in terms of the speed by Eq. (7):

$$T_o - T_c = (D/k_i)(\rho_i q V_g + k_w \nabla T_+) \tag{8}$$

Combining (8) with (2) and (6) we can relate the overall motion to the depth of the groove in (a) the case where the spatial dependence of the nucleation probability is considered and (b) the case where nucleation occurs at one temperature. In the latter case we find

$$V_g = (Ah/\sin\theta)\exp[-C/DV_g] \tag{9}$$

wherein we have taken advantage of the fact that in the experiments under consideration here $\rho_s q V_g \gg k_w \nabla T_+$ and $C = cGk_i/\rho_i q$. Equation (9) shows that at finite speed D depends on V_g transcendentally, but a simple approximation can be obtained by talking the logarithm of Eq. (6): since $\ln V_g$ is slowly varying, we obtain an approximate relation between groove depth, temperature gradient in the water, and interface speed:

$$DV_g \approx \text{const.} \tag{10}$$

4. GROOVES AT MODERATE FREEZING RATES

In the previous section we assume that each layer is completed before the next layer is nucleated, so that the orientation of the groove surface is parallel to the principal crystal plane. We now consider the changes when the slow growth condition no longer holds.

When the nucleation time is shorter than the time for a layer to complete, new layers are successively nucleated on top of uncompleted layers, so that the surface is crossed by a number of steps. The inclination of the surface relative to the limiting $V_g = 0$ orientation, i.e. groove angle θ, is given by the ratio of normal and parallel speeds of the interface. The normal speed V_f is simply related to the nucleation time and the temperature by Eqs. 2 and 3; however, the speed of growth of a layer along the groove is not simply related to τ_p. Consider a layer edge momentarily at an intermediate position z along the facet. The edge moves at a speed controlled by the dissipation of latent heat into the adjacent ice and water, which is proportional to the local temperature difference $T_o - T(z)$. Therefore the growth drive decreases as the edge nears the T_o boundary, and the speed

slows. Hence, the orientation of the surface varies along the depth of the groove; geometrical analysis yields the change in angle

$$\Delta\theta(z) = \tan^{-1}[\, V_f / V_p(z)\,] \tag{11}$$

Thus the surface develops a rounded profile, increasingly rounded near the top of the groove. The theoretical problem of the growth rate belongs to a class of "Stefan problems" dealing with non-steady phase boundary motion in transient thermal fields.[13] Analytic solutions have been obtained for a wide range of problems in one and two dimensions[14] but the specific geometry encountered here has not been addressed.

5. EXPERIMENTAL OBSERVATIONS

Experiments were performed in a vertically oriented Hele-Shaw type cell composed of a pair of transparent 75 mm long by 25 mm wide by 1 mm thick single crystal sapphire windows that are separated by a 0.76 mm thick epoxy-fiberglass composite frame of slightly longer dimension. (The dimensions of the actual cell volume are 70 mm × 20 mm × 0.76 mm.) Individually controlled thermoelectric coolers in thermal contact with the upper and lower 15 mm long by 25 mm wide ends of the windows provide temperature control. Thermistors inserted through the frame edge measure temperatures at two positions near the top and the bottom of the cell, and hypodermic tubes inserted through top and bottom edges of the frame provide liquid and vacuum pump connections. At room temperature only 90% of the cell is filled with deionized, degassed water with the remaining 10% kept empty to provide for the expansion of the contents during freezing and at low pressure to maintain the water in a degassed state. The cell and its thermoelectric coolers are mounted on a temperature controlled heat sink and enclosed in a transparent, dry nitrogen purged chamber that allows viewing of the central 45 mm long by 20 mm wide section of the cell from the front and the rear.

Visual observations are made externally through the front of the chamber with a long working distance video microscope, and recorded on videotape in either real time or time lapse modes. Two zoom lenses provide a continuously adjustable field of view of 1.4 mm to the entire visible portion of the cell with resolutions of 6 μm at the highest magnification (according to the manufacturer and calculated using the standard Rayleigh's criterion) to 70 μm when the entire visible portion of the cell spans the field (limited by the spatial frequency of the 640 × 480 CCD array of the video camera). The cell is illuminated externally through the rear of the chamber with either a 100 W tungsten lamp or a 20 W halogen lamp as the source, depending upon which of two illumination systems is chosen.

The two illumination systems available are lambertian and autocollimator types, and both employ infrared filters to minimize the heat load into the cell. A lambertian type of system, which is a common approach in many experimental investigations, is one in which the emitted or reflected power per unit area of source is the same regardless of direction, and incoherent radiation from any diffuse reflector or scattering surface may be adequately described as lambertian. The lambertian system used here consists of a 100 mm long by 75 mm wide white, diffuse screen just behind the cell that is illumimated by the halogen lamp, and hence every point in the visible portion of the cell is uniformly illuminated with a cone of light having an angular radius of about 22 degrees. By contrast an autocollimator type of system is one in which a point or small extended, incoherent source is imaged at infinity and so the light at any plane short of infinity is uniform in intensity but highly directional. The autocollimator type system used here consists of the tungsten lamp, a ground glass diffuser, an iris diaphragm, a 25 mm diameter, 25 mm focal length plano-convex lens, a 25 mm diameter, a 100 mm focal length plano-convex lens, and a front surface gold mirror. The iris simultaneously controls the intensity and the angular diameter of the cone of light illuminating each point in the visible part of the cell. The minimum acceptable intensity with the current video camera and a 100 W tungsten lamp corresponds to a light cone angular diameter of less than one half of one degree. With either illumination system, a pair of rotatable, linear polarizing filters, one between the microscope lens and the chamber called the analyzer and the other between the chamber and the illuminator called the polarizer, provide control of the polarization directions of the light that passes through the cell and the light collected by the microscope.

The use of two polarizering filters to investigate a birefringent material such as ice is called polarimetry, and it is used here primarily show the polycrystalline nature of the ice produced within the cell. Birefringence, which means two polarization-dependent refractive indexes, causes interference colors to appear in the light transmitted through the ice and vary in hue as either filter is rotated wherever the crystallographic *c*-axis of the ice is not parallel to the direction of propagation. (The birefringence of the sapphire windows does not affect the video images because their *c*-axes are within 1 degree of their surface normals and thus effectively parallel to the imaging system axis.) Where ice grains overlap the range of colors selected by the analyzer becomes very complicated, and, where the ice does not yet fill the space between the windows, bands of similar color act as indicators of uniform thickness.

With the lambertian illumination system, polarimetry must be used in order to see any of the polycrystalline fabric of the ice in the cell, and even

then, because the birefringence in ice is small, only those grains whose *c*-axis direction differs significantly from that of the imaging system axis produce significant color. Regardless of the colors of the grains, the boundary regions between the grains are invisible with polarimetry unless they overlap with respect to the imaging system axis. This is because the tiny volume between the grains, whether wet or dry, does not significantly affect the polarizations or path lengths of the light transmitted through it and therefore produces no change in color. Where grains overlap, the regions of overlap are only visible by virtue of the proper path lengths within the crystallographic orientations of the two grains forming the boundary. As for the interaction between the grain boundaries and the lambertian illumination system alone, the grain boundaries remain invisible, regardless of orientation. The reason is that the lambertian illumination is diffuse and the thin interfaces between transparent regions of similar refractive index scatter as much light into the imaging system as they do out of it, which results in no net change in image contrast. The primary advantage of the lambertian system is that it can uniformly illuminate the entire visible portion of the cell at one time.

In contrast, the auto-collimator type system can only illuminate about an 8 mm diameter section of the cell at one time, but its advantage is that polarimetry is not required to see the polycrystalline fabric of the ice. A vast majority of the grain boundaries are highly visible, regardless of their orientation and the crystallographic orientation of the grains that form them. This is a direct consequence of the very small angular distribution of the light incident on each point in the field of view. The scattering, or refractive, behaviors of the grain boundaries are no different than when the lambertian system is used, but in this situation more light is scattered out of the imaging system than scattered into it, resulting in a dramatic enhancement in image contrast. In addition to grain boundaries, the visibility of many other features that subtly scatter light, such as the edges of facets, voids, and dislocations, is also enhanced. Polarimetry, where it produces interference color, helps distinguish between true grain boundaries and dislocations because of the enhancment in color contrast that results from a significant reduction in stray white light from adjacent regions of the source. The net result of combining polarimetry with the auto-collimator illumination system has revealed a wealth of detail within the ice and at the ice-water interface in this cell, during steady temperature conditions as well as during growth or melting.

The course of freezing in several runs was recorded on video tape and subsequently studied in detail. The initiation of freezing was followed by rapid growth of a thin film of ice on the lower region of the cooled window. The ice developed needle-like structure and grew as feathery dendrites, and

then evolved to a more oriented structure, with a fairly smooth ice-water interface oriented normal to the direction of advance, and grain boundaries parallel to the temperature gradient. The grooves at the intersection of two grains and the water interface were mostly of the normal curved variety, as described by Eq. (1), but there were also one or more large faceted grooves such as sketched in Fig. 1 and as pictured in Fig. 3. Typical grooves were appreciably asymmetric, with angles $30^\circ < \theta < 45^\circ$. As freezing progressed the grooves usually translated with constant shape and orientation along

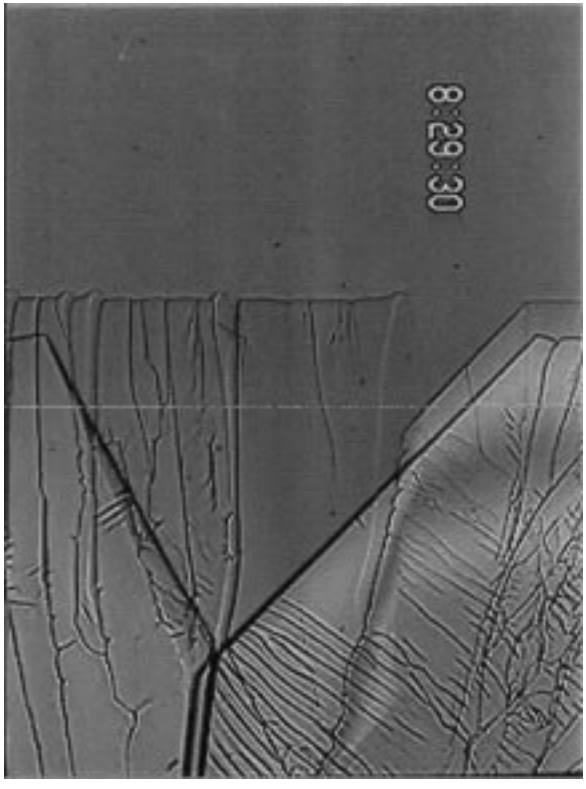

Fig. 3. Photo of an experimental giant faceted grain boundary. Size can be judged by the scale of the rectangular image which is 4.60 mm × 3.46 mm. Ice is growing upward and due to the higher thermal conductivity of the saphire cell windows, there is a deviation from the ideality of the schematic in Fig. 1. We observe "two sheets" each adjacent to the sapphire windows but simply connected by an overall concave region between them. Hence, the "top" giant facet exposes a V shaped region of supercooled water adjacent to the "bottom" sheet which we observe through the groove on the top sheet. The mean ice/water interface on both sheets is the fine dark horizontal line along which $T = T_o$ and where the numerous classical grain boundary grooves on either side terminate.

the direction of the temperature gradient. A record of the trajectory remained as a grain boundary. There were occasional short jogs in the trajectory, but the track usually continued close to the gradient direction for the entire length of the cell. The size of the grooves varied with freezing speed and gradients; the largest being nearly 3 mm deep, as seen in Fig. 3.

6. DISCUSSION

The most striking aspect of crystalline material is its shape. Although equilibrium and growth shapes can be described using thermodynamical and statistical mechanical concepts, a complete description of evolving crystals is challenging and active research area, and one in which John Cahn has made many important contributions. Studies of ice growth have helped to improve the understanding of the general processes of nucleation and growth of crystals. The particular advantages of transparency and convenient temperature range, together with its common occurrence and the variety of natural phenomena, combine to give ice a unique role as a test substance. The morphology of ice crystallization is a distinguishing feature in the different textures of ice occurring in the natural environment, e.g. in frost figures, frozen lakes, glaciers, and sea ice. Many studies have explained the textures in terms of the properties of the material under special conditions.[10, 15–18]

To put into context what we have described here, it is helpful to contrast it with the more commonly studied growth of single crystals, which may take convex shapes or have regions of concavity. Convex single crystals tend to grow in anisotropic forms.[19, 20] Concavities are generally not present on an equilibrium shape, because they increase the chemical potential of the material relative to that of the bulk. However, concavity resulting from instabilities can occur during growth, wherein two regions of a surface advance at a rate that is greater than a region between them. The concavity may persist and thereby characterize the growth form; a common example is that of the snowflake. However, as we have shown here, concavity arises naturally when two or more single crystals grow together. A complex series of competitive phenomena influence the overall growth morphology, and nowhere is this more evident and impressive than in natural ice formations, where polycrystallinity is insured. Hence, the present work suggests that the anisotropic growth of *polycrystalline seeds*, often found in nature, will hold new suprises that can be fruitfully explored using the techniques brought to bear on the study of single crystals.

ACKNOWLEDGMENTS

This research is supported by Army Research Office grants DAAH34-96-1-0433 and DAAH004-96-1-0290, NSF grant OPP95-23513 and ONR grant N00014-94-1-0120.

REFERENCES

1. G. F. Bolling and W. A. Tiller, *J. Appl. Phys.* **31**:1345 (1960).
2. G. E. Nash and M. E. Glicksman, *Phil. Mag.* **24**:577 (1971).
3. R. J. Schaefer, M. E. Glicksman, and J. D. Ayers, *Phil. Mag.* **32**:725 (1977).
4. S. C. Hardy, *Phil. Mag.* **35**:471–484 (1977).
5. P. W. Voorhees, S. R. Coriell, G. B. McFadden, and R. F. Sekerka, *J. Cryst. Growth* **67**:425–440 (1984).
6. L. A. Wilen and J. G. Dash, *Science* **270**:1184–1186 (1995).
7. W. K. Burton, N. Cabrera, and F. C. Frank, *Phil. Trans. Roy. Soc. A* **243**:299–358 (1951).
8. J. W. Cahn, *Acta Metall.* **8**:534–562 (1960).
9. J. W. Cahn, W. B. Hillig, and G. W. Sears, *Acta Metall.* **12**:1421–1439 (1964).
10. W.B. Hillig, in *Growth and Perfection of Crystals*, R. H. Doremus, B. W. Roberts, and D. Turnbull, eds. (Wiley, New York, 1958), pp. 350–360.
11. D. Turnbull, in *Solid State Physics*, Vol. 7, F. Seitz and D. Turnbull, eds. (Academic Press, New York, 1956), pp. 226–308.
12. P. R. Pennington, S. F. Ravitz, and G. Abbaschian, *Acta Metall.* **18**:943–953 (1970).
13. H. W. Carslaw and J. C. Jaeger, *Conduction of Heat in Solids*, 2nd ed. (Oxford, Clarendon Press, 1959).
14. A. M. Meirmanov, *The Stefan Problem* (W. de Gruyter, Berlin/New York, 1992).
15. J. Bilgram, H. Wenzl, and G. Mair, *J. Cryst. Growth* **20**:319–321 (1973).
16. S. C. Colbeck, CRREL Rpt 92-3 (Cold Regions Research and Engineering Lab, Hanover, New Hampshire, 1992).
17. M. Elbaum and J. S. Wettlaufer, *Phys. Rev. E* **48**:3180–3183 (1993).
18. M. G. Worster and J. S. Wettlaufer, *J. Phys. Chem. B* **101**:6132–6136 (1997).
19. J. E. Taylor, J. W. Cahn, and C. A. Handwerker, *Acta Metall.* **40**:1443–1474 (1992).
20. J. S. Wettlaufer, M. Jackson, and M. Elbaum, *J. Phys. A* **27**:5957–5967 (1994).